Multimodal MR imaging of acute and subacute experimental traumatic brain injury: Time course and correlation with cerebral energy metabolites

Marc Maegele[1,2,*], Ewa K Stuermer[2,*], Alexander Hoeffgen[3], Ulla Uhlenkueken[4], Angelika Mautes[5], Nadine Schaefer[2], Marcela Lippert-Gruener[6], Ute Schaefer[7] and Mathias Hoehn[4,8]

Abstract

Background: Traumatic brain injury (TBI) is one of the leading causes of death and permanent disability world-wide. The predominant cause of death after TBI is brain edema which can be quantified by non-invasive diffusion-weighted magnetic resonance imaging (DWI).

Purpose: To provide a better understanding of the early onset, time course, spatial development, and type of brain edema after TBI and to correlate MRI data and the cerebral energy state reflected by the metabolite adenosine triphosphate (ATP).

Material and Methods: The spontaneous development of lateral fluid percussion-induced TBI was investigated in the acute (6 h), subacute (48 h), and chronic (7 days) phase in rats by MRI of quantitative T2 and apparent diffusion coefficient (ADC) mapping as well as perfusion was combined with ATP-specific bioluminescence imaging and histology.

Results: An induced TBI led to moderate to mild brain damages, reflected by transient, pronounced development of vasogenic edema and perfusion reduction. Heterogeneous ADC patterns indicated a parallel, but mixed expression of vasogenic and cytotoxic edema. Cortical ATP levels were reduced in the acute and subacute phase by 13% and 27%, respectively, but were completely normalized at 7 days after injury.

Conclusion: The partial ATP reduction was interpreted to be partially caused by a loss of neurons in parallel with transient dilution of the regional ATP concentration by pronounced vasogenic edema. The normalization of energy metabolism after 7 days was likely due to infiltrating glia and not to recovery. The MRI combined with metabolite measurement further improves the understanding and evaluation of brain damages after TBI.

[1]Department of Traumatology, Orthopedic Surgery and Sporttraumatology, Cologne-Merheim Medical Center (CMMC), University of Witten-Herdecke, Campus Cologne-Merheim, Germany
[2]Institute of Research in Operative Medicine, University of Witten-Herdecke, Campus Cologne-Merheim, Germany
[3]Department of Anaesthesiology and Intensive Care Medicine, Hospital Gummerbach, Gummersbach, Germany
[4]In-vivo-NMR Laboratory, Max-Planck-Institute for Neurological Research, Cologne, Germany
[5]Institute for Neurosurgical Research, Department of Neurosurgery, University of Saarland, Homburg, Germany

[6]Center for Neurosurgery, University of Cologne, Cologne, Germany
[7]FE Experimental Neurotraumatology, Department of Neurosurgery, Medical University Graz, Graz, Austria
[8]Department of Radiology, Leiden University Medical Center, Leiden, Netherlands

*Equal contributors.

Corresponding author:
Ewa K Stuermer, Institute for Research in Operative Medicine, Faculty of Health – School of Medicine Witten/Herdecke University, Cologne D-51109, Germany.
Email: ewa.stuermer@uni.wh.de

Introduction

Traumatic brain injury (TBI) is one of the leading causes of death and permanent disability worldwide. Each year 1.1 million Americans are treated in emergency departments, 50,000 die, and another 235,000 are hospitalized for non-fatal TBI (1). The prevalence of disability following hospitalization with TBI is 3.2 million in America (1,2).

The predominant cause of death and long-term disability after TBI is brain edema (3,4) which can be analyzed by magnetic resonance imaging (MRI). Non-invasive diffusion-weighted MRI (DWI) quantifies the diffusion of water in the brain associated with edema (5,6) and contributes essentially to the understanding of stroke and stroke-related cerebral edema formation (4,7). The use of DWI offers the opportunity to identify the predominant edema type after TBI and, in this way, to distinguish between vasogenic and cytotoxic edema (4,8).

MRI is further applied to evaluate post-lesion events and changes in TBI induced by lateral-fluid percussion (LFP) (9,10). To detect diffuse lesions without hemorrhage, T2-weighted (T2W) MRI has been proven superior over computed tomography (CT) (11). T2W MR data of cortical lesions can be correlated with histologic lesion volume, neurofunction, and allow a distinction of mild and severe TBI of rats (9,10). Furthermore, this multiparametric quantitative MRI show the potential to predict the functional and histopathological outcome for 6 and 12 months after injury (12,13) and findings can be correlated with the state of cerebral energy metabolites of focal and diffuse TBI (14,15).

Although many studies have investigated the formation of brain edema in experimental and clinical settings by DWI, the underlying mechanisms remain poorly defined and the findings and opinions remain heterogeneous in respect to the predominance of cytotoxic or vasogenic form of traumatic brain edema (4,8,10,15). Therefore, the purpose of the present study was to provide a better understanding of the early onset, time course, spatial development, and type of brain edema (i.e. cytotoxic vs. vasogenic) after TBI. Furthermore, the study aimed at the correlation between MRI data and the cerebral energy state which is reflected by the metabolite adenosine triphosphate (ATP). Additional insight was gained when combining perfusion-weighed imaging (PWI), TWW MRI, and histopathology in defined brain regions (regions of interest [ROI]).

Material and Methods

Animals and experimental protocol

All experimental procedures were approved by the local authorities (LA NUVS; NRW; AZ: 23.303-K-K4, 28/ 99). Male Sprague-Dawley rats (weight, 300–350 g; $n = 12$; Harlan Winkelmann, Borchen, Germany) were kept in individual cages for a minimum of 7 days prior to any experimentation. Body weights were assessed at baseline (24 h prior to injury), immediately prior to injury, and then daily after injury until the animals were sacrificed according to their scheduled survival time. Animals were randomly assigned to one of the following three experimental groups: (i) trauma induction and MRI after 4, 5, and 6 hours, followed by substrate-specific bioluminescence imaging and histological evaluation after 6 h ($n = 4$); (ii) trauma induction and MRI after 48 hours, bioluminescence imaging and histological evaluation after 48 h ($n = 4$); and (iii) trauma induction and MRI after 7 days, bioluminescence imaging and histological evaluation after 7 days ($n = 4$).

We have used the LFP brain injury model, as described previously (16), being one of the most widely used and well characterized models of experimental TBI (17). The pressure pulse was measured extracranially by a transducer (Gould Laboratories, Pitman, NJ, USA), integrated in the impact device and recorded on a computer oscilloscope emulation program (R.C. Electronics Inc., Santa Barbara, CA, USA). The trauma induction was performed at a predefined moderate level (2.1 +/– 0.2 atm) in order to achieve moderate to mild brain damage (16,17).

Neurofunctional assessment and composite neuroscore (NS)

The blinded evaluation of neuromotor impairment and recovery after LFP was achieved using a composite neuroscore test, as described previously (16,18). The scores are averaged, and a composite neurological motor score (0–28) is calculated for each animal from the summation of individual test scores. Baseline composite neuromotor scores were calculated 24 h prior to injury. The degree of acute neurological impairment after trauma and recovery was assessed at 24 h and 7 days after impact.

MRI

Animals were intubated, mechanically ventilated, and anesthetized with halothane (1%) in the inhalation gas mixture (70% N_2O, 29% O_2). All MRI measurements were performed in a 4.7T dedicated experimental animal scanner (BioSpec 47/30, Bruker BioSpin, Ettlingen, Germany), equipped with actively shielded gradient coils (100 mT/m; rise time <250 µs). RF transmission was achieved with a 12 cm diameter Helmholtz coil, and signal detection with a 22 mm diameter surface coil, positioned above the skull of the animal. The RF

coils were decoupled from each other: the Helmholtz coil actively, and the receiver coil passively. Gradient echo fast imaging pilot scans were used for accurate positioning of the animal's head in the magnet. T2W images were acquired with a multi-slice multi-echo Carr-Purcell-Maiboom-Gill spin echo sequence: repetition time (TR), 3 s; echo time (TE), 12.5 ms; 16 echoes; field of view (FOV), 4×4 cm^2; matrix, 128×128; slice thickness, 1.21 mm; interslice distance, 1.75 mm. Eight coronal slices were recorded, covering a volume extending 10 mm in the rostrocaudal direction, centered around the cortical lesion.

DWIs were recorded with a multi-slice Stejskal-Tanner spin echo sequence: TR/TE, 2325/35.2 ms; FOV, 4×4 cm^2; matrix, 128×128; slice thickness, 1.21 mm; interslice distance, 1.75 mm. Data were collected for two b-values: 30 and 1500 s/mm^2. Images were recorded for the same coronal slice positions, chosen for T2W images.

Perfusion-weighted imaging (PWI) was performed with arterial spin labelling (labelling time, 3 s). During the first acquisition, arterial spins flowing through the neck were inverted adiabatically (tagging) and the inflow of labelled spins was detected with a SNAPSHOT FLASH imaging sequence (19): TR/TE, 8.9/5.3 ms; FOV, 4×4 cm^2; matrix, 128×64; slice thickness, 2 mm. The second acquisition left the inflowing spins undisturbed by changing the sign of the frequency offset (untagged image). Eight tagged and untagged images each were averaged to improve the signal-to-noise ratio. PWI was recorded in eight coronal slices thus covering the region of cortical lesion and the surrounding area.

For each of the three pre-defined survival groups (6 h, 48 h, and 7 days) a representative animal was depicted with the quantitative T2 and ADC maps, the T2W, DWI, and PWI as well as ATP distribution.

Image calculation and analysis

PWIs were calculated by subtracting the averaged tagged image from the averaged untagged image using homemade software written in IDL (Research Systems Inc., Boulder, CO, USA). For compensation of signal loss caused by the use of the surface receiver coil, the difference image was then divided by the averaged untagged image. Quantitative maps of the ADC were calculated pixelwise based on the monoexponential intravoxel incoherent motion model (5), while T2 maps were calculated from the 16 acquired echoes. For parameter map (T2 and ADC, respectively) calculations the algorithms were applied as described before (7).

ROIs for the MRI parameters and the ATP-specific bioluminescence images were selected in the cortex (1 mm^2), thalamus (1 mm^2), and hippocampus (whole area). The cortical ROI was placed in the center of the cortical lesion. ROI analysis was carried out in the affected, traumatized left hemisphere and in the contralateral non-traumatized right hemisphere, using the image analysis software ImageJ (Rasband, W.S., ImageJ, NIH, http://rsb.info.nih.gov/ij). To ensure the exact placement, all ROIs were selected and measured based on histological findings. Based on the stereotaxic atlas of the rat brain by Praxinos and Watson (20) the best fitting histological sections, bioluminescence and MR images were selected for analysis. Then, the ROIs were identified in the histological section and transferred to the MR image and the bioluminescence image. The procedure was executed blinded by an experienced radiologist.

Histology and bioluminescence imaging

At the end of the MRI measurements, the rat brains were frozen using the funnel freezing method with liquid nitrogen (21). Coronal 20 μm thick sections were cut in a cryostat (CM1850 UV, Leica Biosystems Nussloch GmbH, Nussloch, Germany) at $-20°$C. Alternate sections were used for imaging the ATP concentration and for Hematoxylin-Eosin (HE) staining. Sections intended for bioluminescence were freeze-dried for 24 h at $-20°$C. ATP-specific bioluminescence reaction was carried out as described previously (22).

Statistical analysis

Statistical analysis was performed with SPSS statistical software (SPSS Inc., Chicago, IL, USA). Significant differences were tested using the percentage difference of the ROI values in cortex, hippocampus, and thalamus of the left and right hemisphere using Student's t-test. Composite neuroscore (NS) scores are expressed as means $\pm$ standard deviation (SD) and subjected to a two-way ANOVA followed by a post-hoc Bonferroni correction. Statistical significance was set at $P < 0.05$.

Results

All 12 animals survived the initial TBI via LFP and could be subjected to MRI and subsequent analysis. On average, animals lost about 10% of their initial body weight during the first 2 days after impact, but had recovered up to around 97 percent of their initial body weight at day 7 after injury (data not shown).

Composite neuroscore (NS)

No differences were observed in the NS among intact rats prior to injury with respect to forelimb flexion, lateral pulsion, hind limb function, and baseline

angles in the angle-board test. At 24 h post-injury a significant level of severe neurological impairment was detected in all animals ($P < 0.005$). Recovery of neuromotor function started during the first week post-injury. Animals that survived for 7 days post injury ($n = 4$) had regained some neuromotor function when tested for forelimb flexion, lateral pulsion, hind limb function, and baseline angles in the angle-board test at 1 week after impact (Fig. 1).

Regional MRI parameter variations and ATP concentrations

T2W hyperintensity and, therefore, quantitative T2 value increase was observed in all selected ROIs. This T2 enhancement was most pronounced at acute and subacute time points with maximum at 48 h after TBI (Fig. 2). On day 7 after injury, this effect was hardly distinguishable and only a slight enhancement in T2 signal intensity remained visible. Relative T2 increased above the values of the contralateral non-injured hemisphere (Fig. 3); corresponding values are listed in Table 1 for all ROIs at all time points studied. T2 values were found to be statistically significant from those of the contralateral non-injured hemisphere for the cortex and thalamus at acute (6 h) and subacute (48 h), and for the hippocampus at subacute time points ($P < 0.05$).

DWI and ADC mapping

On the ADC images, no clearly distinguishable lesion area could be observed. Upon visual inspection no homogeneous area of ADC alteration between both hemispheres was found in any of the selected ROIs and at any time point studied (Fig. 2). ROI analysis showed that ADC values scattered widely in the lesioned areas. In some cases, this also resulted in variable values in neighboring slices of the same animal (data not shown). This situation of extreme ADC heterogeneity is reflected in the large standard deviation of the ADC changes, in all ROIs and at all time points studied (Fig. 3, Table 1). Quantitative analysis led to rather small changes in ADC values with high standard deviation due to variations across slices. No statistical significance or even a clear trend towards increased or decreased values as compared to non-injured contralateral hemispheres was detected for all ROIs at all time points studied.

PWI

PWI led to clearly detectable perfusion alterations in the traumatic hemisphere (Fig. 2). Relative to the contralateral non-injured cortex, the values decreased to almost 20% of normal in the acute phase within the injured ipsilateral cortex (4–6 h post injury; $P < 0.05$). The tissue perfusion showed a very pronounced increase above reference by almost 50% at 48 h after injury ($P < 0.05$), before decreasing again by about 15% relative to reference at day 7 (Fig. 3, Table 1). This pattern of reduction in the acute phase, followed by an increase in the subacute phase (48 h post injury) and then again a decrease in the chronic phase at day 7 after injury is paralleled but by far less pronounced and non-significant
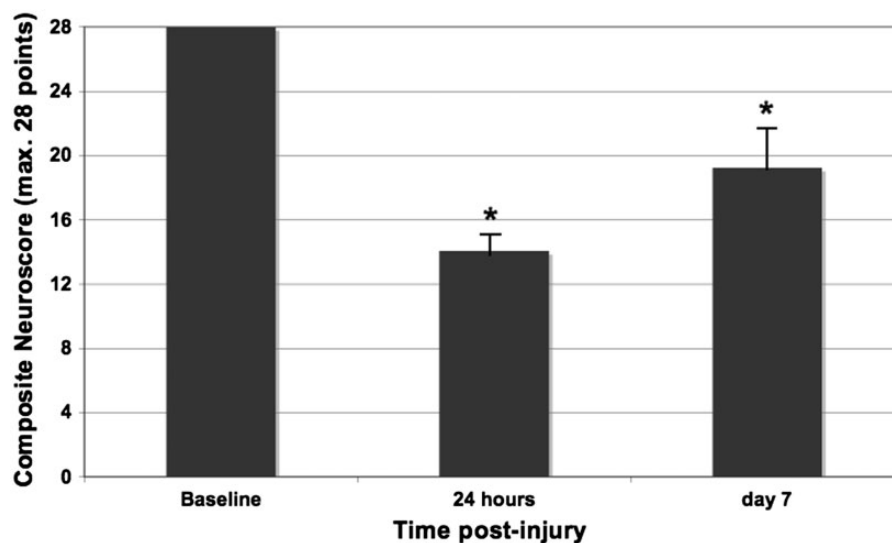

Fig. 1. Results of the composite neuroscores (NSs) assessed at baseline, at 24 h, and at day 7 after injury. Significant reduction of neuromotor function after TBI; recovery of some neuromotor function at 1 week after impact. Values are expressed as means; $P < 0.05$ was considered as statistically significant.
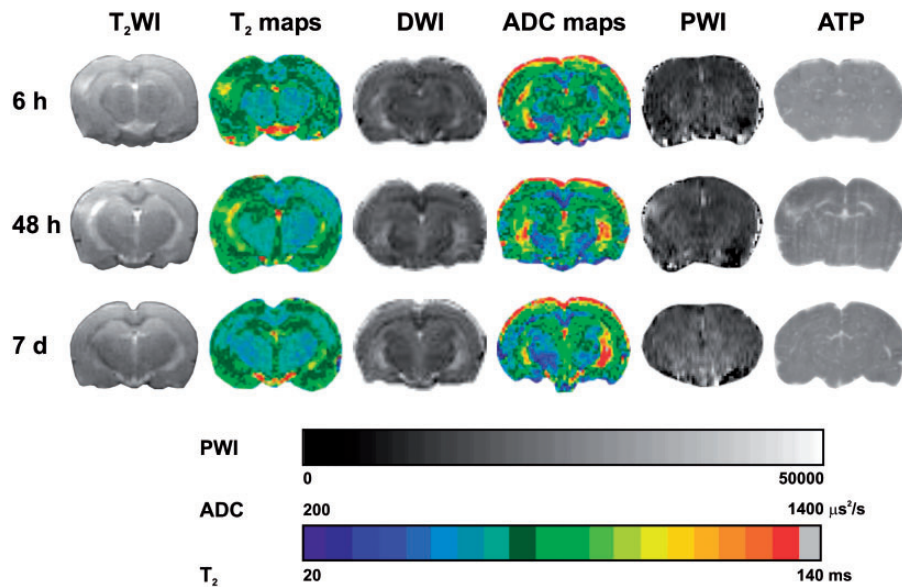
Fig. 2. Exemplar regional MRI parameter distributions and ATP concentration. Multiparameter presentation of the LFP induced TBI in the rat. MRI parameters T2, ADC, DWI, and PWI are depicted together with bioluminescence imaging showing the regional ATP distribution at the endpoint of the corresponding *in vivo* study. One representative animal from three different survival groups was chosen for depiction of the time dependent changes of the pathophysiological processes. Perfusion images show a transient hyper-perfusion in the lesioned cortex at 48 h. ATP images indicate small and transient reduction of the ATP level at the early time points at 6 h and 48 h only.
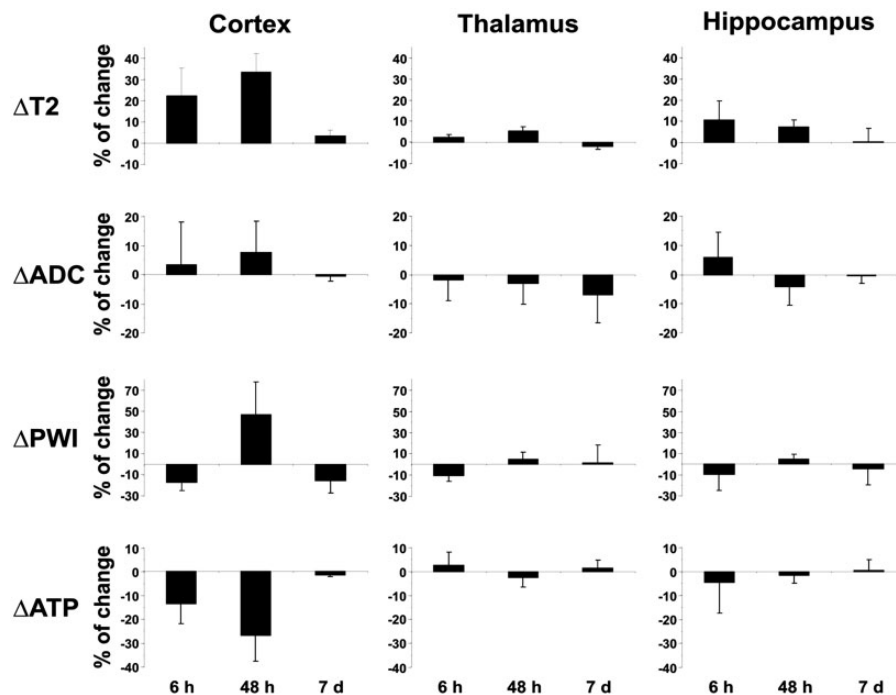

Fig. 3. Quantitative evaluation of MRI parameter and ATP changes for all ROIs at 6 h, 48 h, and at day 7 post injury. Quantitative evaluation of the parameter changes in percent (%) relative to the homotopic region in the contralateral non-injured hemisphere. T2 values were statistically significant from those of the contralateral non-injured hemisphere at all time points except at day 7 post injury. Values are expressed as means; $P < 0.05$ was considered as statistically significant.

Table 1. Parameter changes in traumatically lesioned hemispheres relative to contralateral uninjured hemispheres in percent for selected ROIs at all studied time points. Values are expressed as mean ± SD; *P < 0.05 was considered as statistically significant (between both hemispheres).

	Time after injury	ΔT_2	ΔADC	ΔPWI	ΔATP
Cortex	4 h	17.82 ± 10.71*	−2.52 ± 8.35	−11.35 ± 15.61	−
	5 h	21.49 ± 12.19*	3.96 ± 11.67	−19.14 ± 26.02	−
	6 h	22.32 ± 13.19*	3.38 ± 14.51	−17.29 ± 7.13*	−13.32 ± 8.36*
	48 h	33.35 ± 8.9*	7.7 ± 10.69	46.54 ± 30.8*	−26.72 ± 10.8*
	7 days	3.57 ± 2.77	−0.48 ± 1.86	−15.04 ± 12.14*	−1.51 ± 0.42*
Thalamus	4 h	2.95 ± 0.98*	−1.5 ± 8.47	−9.73 ± 4.6*	−
	5 h	2.5 ± 0.48*	−6.58 ± 11.41	−24.86 ± 23.86	−
	6 h	2.32 ± 1.32*	−1.73 ± 7.27	−10.25 ± 5.48*	2.68 ± 5.44
	48 h	5.44 ± 1.96*	−3.16 ± 6.98	4.55 ± 7.16	−2.38 ± 4.17
	7 days	−2.09 ± 1.37	−7.04 ± 9.52	1.41 ± 16.67	1.58 ± 3.37
Hippocampus	4 h	9.18 ± 6.2	−3.52 ± 8.7	−4.57 ± 3.34*	−
	5 h	9.49 ± 8.18	1.56 ± 4.87	−11.51 ± 6.87*	−
	6 h	10.76 ± 8.98	5.85 ± 8.54	−9.41 ± 15.12	−4.55 ± 12.88
	48 h	7.45 ± 3.15*	−4.27 ± 6.27	5.09 ± 15.12	−1.58 ± 3.23
	7 days	0.38 ± 6.26	−0.34 ± 2.74	−4.29 ± 14.86	0.59 ± 4.56

changes in the two other ROIs, i.e. the thalamus and the hippocampus.

ATP imaging for energy metabolism

A pronounced reduction in the ipsilateral cortical ATP content of down to almost 30% relative to the contralateral non-injured hemisphere was observed within the acute (6 h) and subacute phases (48 h) post injury (Figs. 2, 3; Table 1). At day 7 after injury no relevant ATP reduction was detectable. The changes in ATP content in the two other ROIs, i.e. the thalamus and the hippocampus, were much less pronounced and non-significant in both the acute and subacute phases after injury as compared to the cortex. Normalization on day 7 after injury was observed in both ROIs to the same pattern as in the cortex.

Correlation of MR findings and cerebral energy state

The comparison of T2W images and cerebral ATP concentration led to a correlation between these two variables. Both parameters displayed coupled time course behavior. The correlation coefficients were $R^2 = 0.2876$ at 6 h post injury, $R^2 = 0.3859$ at 48 h post injury, and $R^2 = 0.0286$ at day 7 post injury, respectively. Due to the large variability of ADC values no correlation of this MRI parameter with the energy metabolic state of the tissue was calculated.

Histopathological examination

Histopathological evidence of tissue damage was predominantly seen in the ipsilateral cortex and corpus callosum (Fig. 4). The damaged cortex showed areas of deformation with infiltration of small microglia-like cells, with only limited evidence of any hemorrhage. Also, in the hippocampus and thalamus, there was evidence of neuronal loss in combination with infiltration of similar microglia-like cells (data not shown). In detail, the histological analysis which was performed 6 h after TBI showed an involvement of the cortex and the underlying white substance including the alveus of the hippocampus. The white substance showed tears. The maximal affected cortical area was pale. In lamina II–IV, Nissl substance and nucleoli were out of detection range. Thus, neurons could not be identified. Forty-eight hours after TBI the structure of the affected cortical area did not show significant changes. In all lamina (I–IV) an enhancement of small cell nuclei, presumably astrocytes, could be detected. Because of soaring tears the compactness of the white substance seemed to be dissolved. In the hippocampus formation the alveus was increasingly impaired and the Ammon's horn showed less cell density. In contrast, the involved cortical area could not be exactly identified because of the high cell density seven days after TBI (Fig. 4). Compared to the contralateral cortex, the number of neurons seemed to be lower and no vertical cell columns were observed in the deeper lamina.
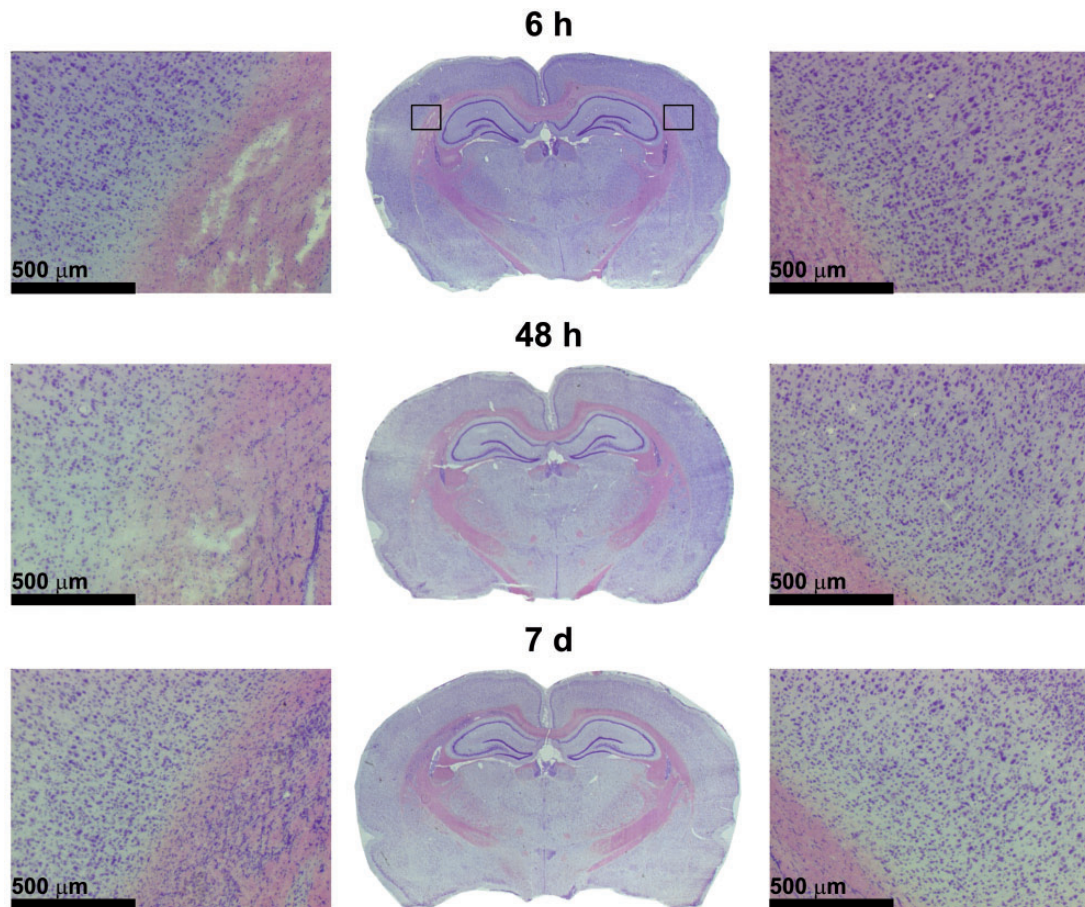
Fig. 4. Representative HE-stained coronal brain sections for three survival time points. The mid-column shows complete coronal brain sections through the center of the inflicted lesion. The cortical ROIs for both injured (left) and non-injured hemispheres (right) are exemplified for the section obtained at 6 h after impact and are depicted in the upper-central panel. The two lateral columns show higher magnifications of the indicated ROIs. The tissue damage was predominantly seen in the corpus callosum and ipsilateral cortex. The latter showed areas of deformation with infiltration of small microglia-like cells, with only limited evidence of any hemorrhage.

Massive infiltrates of small cells in the white substance below the cortical damage were striking. These findings corresponded well to the signal intensity changes seen in T2 maps at the same neuroanatomical level.

Discussion

In the last decade, bioenergetic behavior as a marker in monitoring disease development and drug effect was focused to receive more information of (sub)cellular bioenergetics in the brain. Metabolic changes during brain hypoxia resulted in energetic failure and subsequently in neuronal dysfunction and membrane breakdown (14,15).

Moderate to mild damage was observed as reflected by transient, but pronounced development of vasogenic edema and perfusion reduction. The heterogeneous ADC patterns indicated a parallel, but mixed expression of vasogenic and cytotoxic edema. When perfusion falls below a critical threshold, cellular energy metabolism is disrupted, ionic membrane pumps fail, and osmotic cellular swelling occurs. The dynamic process of a moderate edema development is reflected by the ensuing T2 enhancement which has a pronounced maximum in the cortex at 48 h after TBI. The following decrease at 7 days indicated a resolvement of edema within this week. In the hippocampus and thalamus, a weaker T2 increase was expressed during the first 2 days that completely resolved again after 1 week. T2 enhancement must be interpreted as reflecting a net water increase in the tissue volume under inspection. This came about by vasogenic edema formation due to blood–brain barrier disturbance but might also be affected by water accumulation in cystic structures within glial conversional processes. While ipsilateral thalamus and hippocampus remained widely, but not completely, unaffected, it would be highly interesting to study how the severity of tissue damage in the cortex

and more widespread in deeper brain structures would be influenced by a stepwise increase of the percussion impact intensity.

All these results corresponded with recent studies of Albensi (23) and Alsop (11), and indicated that the time course of T2 enhancement for the moderate fluid percussion injury had indeed two maxima at 24 h and 48 h after TBI. This probably demonstrated the edema formation and – after resolvement of the edema and consequent T2 normalization - a further enhancement 2 weeks after TBI showing glial alterations and cyst formation, accompanied by secondary T2 increase, in full analogy with the cystic transformation after ischemic insult (24). Previous reports from our group also show evidence of glial alterations and cyst formation 2 weeks after moderate fluid percussion injury (18,25).

Brain edema is defined as an abnormal accumulation of fluid within the brain parenchyma. When it occurs as a consequence to blood-brain barrier disturbance, it has been classified as vasogenic edema (4,26). It is a common problem in cerebral ischemia in which a disturbance or breakdown of energy metabolism leads to a breakdown of the ionic homeostasis and a consequent increase of the intracellular fluid content (4,7,8). DWI has been noted to detect the early cascade of ischemic events beginning with the formation of cytotoxic edema with the breakdown of cellular energy metabolism. This process is reflected by a decrease of the apparent diffusion coefficient ADC (7). An increased ADC, on the other hand, is related to vasogenic edema (4,27).

In the present investigation a mixture of vasogenic and cytotoxic edema in parallel may, however, lead to an ADC increase partially compensated by a parallel development of ADC reduction. Depending on the relative pronouncement of these two competing processes, the experimentally observed ADC may become rather heterogeneous with spatial variation between elevated and decreased values. Indeed, recent clinical and experimental studies suggested that the role of vasogenic edema in TBI may have been overemphasized and cytotoxic edema play an important part (4,27). However, this remains controversial: some authors registered an initial increase in ADC after TBI (28–30). Others showed an initially decreased ADC which was followed by increased value (11,23). Therefore, the time course of both edema processes (contributing competitively to the experimentally observed ADC value) may strongly depend on the particular TBI model used and on the lesion severity inflicted by the model.

On perfusion-weighted MR images a perfusion reduction was notable during the first 6 h after TBI followed by a hyperperfusion at 48 h. Seven days after TBI, perfusion was reduced again. Cerebral hypertension is followed by endothelial damage and distribution of vasogenics, which lead to vascular constriction by

vasoactive substances (31,32). This vasoconstriction is, furthermore, associated with an insufficient production of vasodilatating substances (30). Further explanations may be vasospasm following subarachnoidal hemorrhage or vasoactive effects associated with subdural hemorrhage (15), although hemorrhages were not detectable in the MR images and not observed in histology either. Brain edema may also contribute to the reduced cerebral perfusion. It may be assumed that an initial vasoconstriction is followed by a vasodilatation through delayed distribution of vasodilatating agents or vasoparalysis after initial spasm (31).

Pronounced reduction of ATP content was found to be limited to the cortical lesion area within the first 48 h. In the other ispilateral ROIs (thalamus and hippocampus) ATP level was not significantly reduced at any time. As the cortical ATP reduction occurred in parallel with the development of the vasogenic edema with its strongest expression at 48 h, it may safely be assumed that part of this ATP reduction was actually due to some moderate brain swelling which would result in an apparent dilution of the substrate ATP (lesser cells per unit volume) (31). Nevertheless, this dilution would not account for the whole reduction, but some loss was observed. Cell death due to an ischemic situation, is unlikely a perfusion reduction of about 20% of higher relative to the normal, contralateral hemisphere. This reduction in blood flow did not lead to serious tissue damage and thus cannot alone explain a lowered ATP level. This ATP reduction could be transient only, and full recovery may be in parallel with the resolution of the edema. Alternatively, and more likely, the glial scar formation, as seen on the histological sections, might lead to a (partial) cell volume replacement of the neurons lost in the wake of the percussion. Thus, the invading microglia may compensate the ATP content in the ROI under investigation thus falsely indicating that a normal ATP content reflects a full neuronal tissue recovery.

If the additional measurement of energy metabolism may thus contribute to the exact differentiation between the two types of edema remains still speculative and warrants further investigation. Clinically, the imaging distinction between vasogenic and cytotoxic edema can be very useful in disorders where both coexist. Distinguishing vasogenic edema from cytotoxic edema in these disorders may be important for determining patient prognosis after appropriate therapy. Diffusion properties can aid in differentiating these two entities since vasogenic edema, characterized by an increase in more mobile extracellular water, results in elevated ADC, while the cytotoxic edema, for example after ischemia, exhibits reduced ADC. It is noteworthy, that vasogenic edema may sometimes appear slightly hyper intense on DWI, despite the elevation of

ADC, due to T2 shine-through effects, again illustrating the increased specificity of ADC maps for true reduced diffusion.

We are aware of some limitations in this study. The apparent strength of ADC being highly sensitive to both vasogenic and cytotoxic edema resulted in highly heterogeneous pattern of expression of both edematous tissue regions. It would have been interesting to follow the development and/or resolution of these edema types over time. For this analysis, intra-individual longitudinal recording of highly resolved ADC together with careful image mapping onto a standardized, high-resolution rat brain template would be necessary. However, as different cohorts of animals were used for different survival times after lesion impact, such longitudinal, spatio-temporal analysis of the ADC changes have not been possible. A similar limitation is related to the correlation of the anatomical tissue damage on histological sections with the MRI alterations. However, histological staining had to be performed on frozen tissue sections due to the necessary funnel freezing to preserve the *in vivo* metabolic state of the brain. The consequent lower histological quality made detailed regional correlation with T2 changes on MR images impossible. Future studies will be designed to provide intra-individual longitudinal studies of repetitive MRI including endpoint correlation with high quality histological staining obtained after perfusion fixation of the brains.

In conclusion, in our model of LFP-induced TBI we have described for the first time regionally highly heterogeneous distribution of vasogenic and cytotoxic edema, as reflected by the patchy patterns of increased and decreased ADC values, respectively. Regional distribution of T2 relaxometric changes were found to agree well with histological tissue damage in cortex, thalamus, and hippocampus. Interestingly, breakdown of energy metabolism shown to be only transient within the 1 week observation period must be cautiously interpreted as due to glial formation in these regions but not full neuronal recovery. Future longitudinal studies will be able to build on the present findings to further unravel the regionally heterogeneous edema development and cell death.

References

1. Corrigan JD, Selassie AW, Orman JA. The epidemiology of traumatic brain injury. J Head Trauma Rehabil 2010; 25:72–80.
2. Zaloshnja E, Miller T, Langlois JA, et al. Prevalence of long-term disability from traumatic brain injury in the civilian population of the United States in 2005. J Head Trauma Rehabil 2008;23:394–400.
3. Marmarou A, Fatouros PP, Barzo P, et al. Contribution of edema and cerebral blood volume to traumatic brain swelling in head-injured patients. J Neurosurg 2000;93: 183–193.
4. Unterberg AW, Stover J, Kress B, et al. Edema and brain trauma. Neurosci 2004;129:1021–1029.
5. Le Bihan D, Breton E, Lallemand D, et al. Magnetic resonance imaging of intravoxel incoherent motions application to diffusion and perfusion in neurologic disorders. Radiology 1986;161:401–407.
6. Schaefer PW, Grant PE, Gonzalez RG. Diffusion-weighted MR imaging of the brain. Radiology 2000; 217:331–345.
7. Hoehn-Berlage M, Norris DG, Kohno K, et al. Relationship of quantitative diffusion NMR imaging with blood flow, energy metabolism and tissue pH in focal cerebral ischemia of rat. J Cereb Blood Flow Metab 1995;15:S62–65.
8. Huisman T. Diffusion-weighted imaging: basic concepts and application in cerebral stroke and head trauma. Eur Radiol 2003;13:2283–2297.
9. Kharastishvili I, Sierra A, Immonen RJ, et al. Quantitative T2 mapping as a potential marker for the initial assessment of the severity of damage after traumatic brain injury in rat. Exp Neurol 2009;217:154–164.
10. Lescot T, Fulla-Oller L, Po C, et al. Temporal and regional changes after focal traumatic brain injury. J Neurotrauma 2010;27:85–94.
11. Alsop DC, Murai H, Detre JA, et al. Detection of acute pathologic changes following experimental traumatic brain injury using diffusion-weighted magnetic resonance imaging. J Neurotrauma 1996;13:515–521.
12. Immonen RJ, Kharastishvili I, Groehn H, et al. Quantitative MRI predicts long-term structural and functional outcome after experimental traumatic brain injury. Neuroimage 2009;45:1–9.
13. Li YH, Wang JB, Li MH, et al. Quantification of brain edema and hemorrhage by MRI after experimental traumatic brain injury in rabbits predicts subsequent functional outcome. Neurol Sci 2012;33:731–740.
14. Pascual JM, Solivera J, Prieto R, et al. Time course of early metabolic changes following diffuse traumatic brain injury in rats as detected by (1)H NMR spectroscopy. J Neurotrauma 2007;24:944–954.
15. Xu S, Zhou J, Racz J, et al. Early microstructural and metabolic changes following controlled cortical impact injury in rat: a magnetic resonance imaging and spectroscopy study. J Neurotrauma 2011;28:2091–2102.
16. McIntosh TK, Vink R, Noble L, et al. Traumatic brain injury in the rat - characterization of a lateral fluid-percussion model. Neurosci 1989;28:233–244.
17. Thompson HJ, Lifshitz J, Marklund N, et al. Lateral fluid percussion brain injury: A 15-year review and evaluation. J Neurotrauma 2005;22:42–75.
18. Maegele M, Lippert-Gruener M, Ester-Bode T, et al. Reversal of neuromotor and cognitive dysfunction in an enriched environment combined with multimodal early onset stimulation after traumatic brain injury in rats. J Neurotrauma 2005;22:772–782.
19. Kerskens CM, Hoehn-Berlage M, Schmitz B, et al. Ultrafast perfusion-weighted MRI of functional brain activation in rats during forepaw

stimulation: Comparison with T*(2)-weighted MRI. NMR Biomed 1996;9:20–23.

20. Paxinos G, Watson C. The Rat Brain in Stereotaxic Coordinates, 6th edn. San Diego, CA: Academic Press, 2007.

21. Ponten U, Ratcheso RA, Salford LG, et al. Optimal freezing conditions for cerebral metabolites in rats. J Neurochem 1973;21:1127–1138.

22. Paschen W. Imaging of energy metabolites (ATP, glucose and lactate) in tissue sections: a bioluminescent technique. Prog Histochem Cytochem 1990;20:1–122.

23. Albensi BC, Knoblach SM, Chew BGM, et al. Diffusion and high resolution MRI of traumatic brain injury in rats: Time course and correlation with histology. Exp Neurol 2000;162:61–72.

24. Wegener S, Weber R, Ramos-Cabrer P, et al. Temporal profile of T2-weighted MRI distinguishes between pannecrosis and selective neuronal death after transient focal cerebral ischemia in the rat. J Cereb Blood Flow Metab 2006;26:38–47.

25. Maegele M, Lippert-Gruener M, Ester-Bode T, et al. Multimodal early onset stimulation combined with enriched environment is associated with reduced CNS lesion volume and enhanced reversal of neuromotor dysfunction after traumatic brain injury in rats. Europ J Neurosci 2005;21:2406–2418.

26. Ito J, Marmarou A, Barzo P, et al. Characterization of edema by diffusion-weighted imaging in experimental traumatic brain injury. J Neurosurg 1996;84:97–103.

27. Muir JK, Boerschel M, Ellis EF. Continuous monitoring of posttraumatic cerebral blood-flow using laser-Doppler flowmetry. J Neurotrauma 1992;9:355–362.

28. Schneider G, Fries P, Wagner-Jochem B, et al. Pathophysiological changes after traumatic brain injury: comparison of two experimental animal models by means of MRI. MAGMA 2002;14:233–241.

29. Long JB, Gordon J, Bettencourt JA, et al. Laser-Doppler flowmetry measurements of subcortical blood flow changes after fluid percussion brain injury in rats. J Neurotrauma 1996;13:149–162.

30. Kimura M, Dietrich HH, Dacey RG. Nitric-oxide regulates cerebral arteriolar tone in rats. Stroke 1994;25: 2227–2233.

31. Thomale UW, Schaser K, Kroppenstedt SN, et al. Cortical hypoperfusion precedes hyperperfusion following controlled cortical impact injury. Acta Neurochir Suppl 2002;81:229–231.

32. Okada Y, Kloiber O, Hossmann KA. Regional metabolism in experimental brain tumors in CATS: relationship with acid/base, water, and electrolyte homeostasis. J Neurosur 1992;77:917–926.